SAND2023-03395C

Proceedings of the ASME 2023
Pressure Vessels & Piping Conference
PVP2023
July 16-21, 2023, Atlanta, Georgia, USA

PVP2023-106417

EFFECT OF HYDROGEN PARTIAL PRESSURE ON FATIGUE CRACK GROWTH RATES OF LOW ALLOY, QUENCHED AND TEMPERED STEELS

Paolo Bortot[1], Matteo Ortolani[1], Chris San Marchi[2], Joseph Ronevich[2]

[1]Tenaris Dalmine, Dalmine, Italy
[2]Sandia National Laboratories, Livermore, CA, USA

ABSTRACT

Low alloy, quenched and tempered Cr-Mo and Ni-Cr-Mo steels are commonly used for construction of seamless pressure vessels for hydrogen gas storage. Designing such vessels for high-pressure gaseous hydrogen service requires knowledge of fatigue crack growth rates and fracture toughness in the service environment at the design pressure. Measurement of these properties is challenging, and only a few laboratories in the world are equipped to make these measurements at very elevated pressure up to 103 MPa (15,000 psi) which are of interests for pressure vessels to be used as buffers in hydrogen refueling stations. In recent years, these properties for common low alloy steels were published in the ASME Boiler and Pressure Vessel Code Case 2938-1, therefore allowing design and construction without the need for dedicated testing. However, the fatigue crack growth rate curves published in the CC were determined from test data at 100 MPa and above and may be over-conservative for lower pressure applications. Prior publication PVP2019-93907 ([1]) in fact, already proposed a correction factor of fatigue crack growth rates based on hydrogen fugacity. Since then, new data were generated at lower pressures i.e. 55 MPa (8,000 psi). This paper presents the new findings and discusses the applicability of the previously proposed equation, which could allow reducing conservatism in current design of pressure vessels.

Keywords: Pressure Vessels Design, Hydrogen Testing

NOMENCLATURE

Q&T	Quenched & Tempered
FCGR	Fatigue Crack Growth Rate
UTS	Ultimate Tensile Strength
HRS	Hydrogen Refueling Station
BPVC	Boiler Pressure Vessel Code
FT	Fracture Toughness
CC	Code Case
OD	Outer Diameter
R	Load Ratio in Fatigue
R^*	Universal Gas Constant
WT	Wall Thickness
YS	Yield Strength
DCPD	Direct current potential drop
LBB	Leak Before Break
FAD	Failure Assessment Diagram

1. INTRODUCTION

Hydrogen is widely considered a key ingredient for carbon-free energy distribution and is typically transported and stored in pressure vessels designed and fabricated using ferritic steels. More specifically, Q&T low alloy Cr-Mo and Ni-Cr-Mo based steels with limited tensile strength (i.e., UTS < 950 MPa) are commonly used.

These technologies have been in place for many decades despite knowledge that ferritic steels suffer from hydrogen embrittlement, resulting in a reduction of ductility and fracture resistance as well as increase of FCGR in case of cyclic services ([2]-[6]). Nowadays, Cr-Mo and Ni-Cr-Mo pressure vessels are extensively used as buffers for HRSs and, as such, are typically subjected to severe fluctuations in pressure, depending on consumers' demand and the number of vehicles being refilled.

Design for hydrogen service is based on the rules given in the ASME BPVC Section VIII Division 3 art. KD-10, requiring both FCGR and FT measurements in the expected service environment with tests conducted on triplicate specimens and three different heats for a full material qualification. In addition, FCGR tests are to be conducted at frequency of 0.1 Hz.

Given the extent of such requirements and the limited testing capabilities and laboratories available worldwide, there have been efforts to produce tests and publish data that could help designers and manufacturers. The recently approved ASME BPVC CC 2938-1 provides design curves, eliminating the need for testing in hydrogen gas of common SA-372 and SA-723 Cr-

Sandia National Laboratories
U.S. DEPARTMENT OF ENERGY NNSA
Sandia National Laboratories is a multimission laboratory managed and operated by National Technology & Engineering Solutions of Sandia, LLC, a wholly owned subsidiary of Honeywell International Inc., for the U.S. Department of Energy's National Nuclear Security Administration under contract DE-NA0003525.

Mo and Ni-Cr-Mo steels, thus offsetting a significant burden for the designer.

These design curves (also known as master curves) describe the behavior of the aforementioned Cr-Mo and Ni-Cr-Mo steels, having tensile strength up to 915 MPa, over a broad range of stress intensity factor ranges (ΔK), providing significant improvement in design life prediction compared to outcomes from previously available data [7]. Two distinct design curves were developed: (1) a comparatively steep power law at low ΔK, and (2) a region of da/dN-ΔK slope consistent with fatigue in air at high ΔK (but with da/dN more than a factor of 10 greater). However, it is important to point out that CC 2938-1 was developed based on FCGR and FT test data generated in 106 MPa pure H_2 ([1], [8]). Although CC 2938-1 is applicable to any lower pressure, this approach is likely overly conservative, as FGCR shows a dependency on test pressure, especially in the low-ΔK regime ([9], [10]).

San Marchi et al. [1] proposed a simple equation to capture the effects of pressure on the da/dN curve, by introducing a square root dependency on the H_2 gas fugacity:

$$\frac{da}{dN} = C\left[\frac{1+C_H R}{1-R}\right]\Delta K^m \left(\frac{f}{f_{ref}}\right)^{½} \quad (1)$$

where C, C_H and m are constants, R is the load ratio (minimum stress intensity factor, K_{min} divided by maximum stress intensity factor, K_{max}), ΔK is the stress intensity factor range (= K_{max} – K_{min}), f is the fugacity of the gaseous hydrogen (thermodynamic pressure) and f_{ref} is a reference fugacity.

Using the Noble-Able equation of state, San Marchi et al. ([11], [12]) developed a simple equation where the fugacity is a function of pressure and temperature:

$$f = P\exp\left(\frac{P\,b}{R^* T}\right) \quad (2)$$

where P is the pressure of interest in MPa, R^* is the universal gas constant (= 8.31447 J mol^{-1} K^{-1}), T is temperature in Kelvin degrees and b is the co-volume constant (equal to 15.84 cm^3/mol for hydrogen). Similarly, the reference fugacity is the thermodynamic pressure at a reference pressure (P_{ref}) of 106 MPa ([1]):

$$f_{ref} = P_{ref}\cdot\exp\left(\frac{P_{ref}\,b}{R^* T}\right) \quad (3)$$

Equation (1) can then be rewritten as:

$$\frac{da}{dN} = C\left[\frac{1+C_H R}{1-R}\right]\Delta K^m\, f(P) \quad (4)$$

where $f(P)$ is expressed by combining equations 2 and 3:

$$f(P) = \left[\left(\frac{P}{P_{ref}}\right)\exp\left(\frac{b}{R^* T}\left(P - P_{ref}\right)\right)\right]^{½} \quad (5)$$

Equation 5 applies only to the power law relationship for the low ΔK regime, whereas in the high ΔK regime, da/dN appears to be relatively insensitive to test pressure and therefore $f(P)$ = 1.

Figure 1 shows the design curves from CC2938-1 (solid line) and application of Equation (4) to predict FCGR data for 55 MPa H_2 gas pressure (dashed line) for three values of R (0.1, 0.5 and 0.7). Only a single curve exists in the upper ΔK region where FCGR is approximated as independent of pressure. The effect of pressure at low ΔK appears relatively small on this log-log plot, however, the predicted number of cycles to failure using the pressure correction is significant for a pressure vessel operating at a maximum pressure of 55 MPa.

The present work shows recently generated FCGR and FT data at 55 MPa H_2 gas pressure. These experimental data are used to assess the validity of the proposed pressure correction (Equation (4)). In addition, the potential benefit arising from the use of pressure-corrected FCGR curves is demonstrated in Section 4, with a simple example comparing the results of a life assessment calculation using the curves from current CC2938-1 and the pressure-corrected da/dN curves (corrected to 55 MPa H_2).

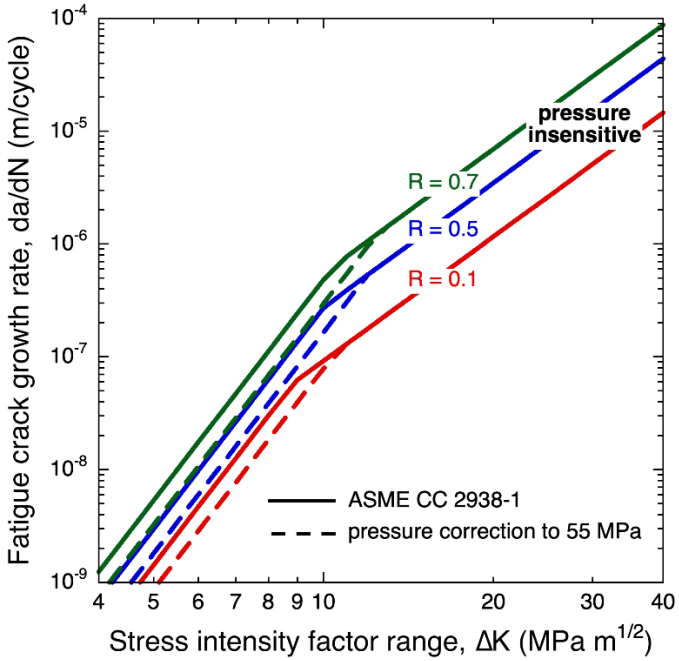

FIGURE 1: EFFECT OF PRESSURE ON FCGR MASTER CURVES AS PER EQUATION (4)

2. MATERIALS AND METHODS

Materials

The investigated material is an ASTM A372 Grade N, Class 100, as per standard specification [13]. Note that this steel is equivalent to the ASME SA-723 Grade 1, Class 1 reported in [1] and [8].

All specimens used were machined from the cylindrical region of an industrially Q&T pressure vessel with size 360 × 55

mm (OD × WT), with YS = 720 MPa and UTS = 870 MPa. After the Q&T heat treatment, the resulting microstructure consisted of uniformly tempered martensite through the thickness, as shown in Figure 2.

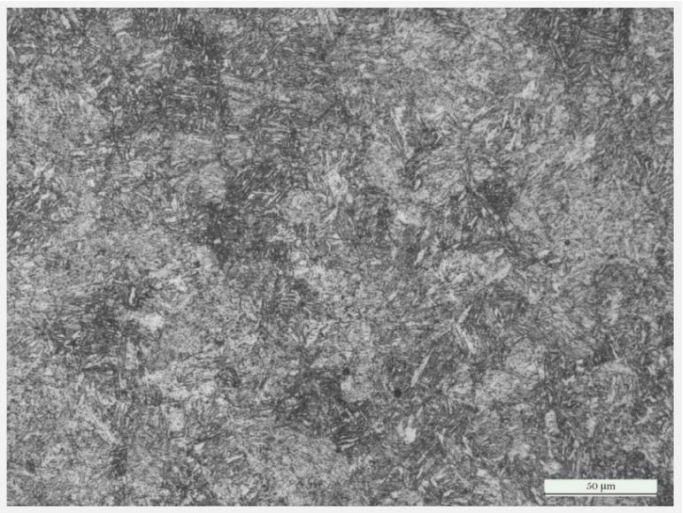

FIGURE 2: Q&T MICROSTRUCTURE FOR A372 GRADE N, CLASS 100 REVEALED WITH 2% NITAL ETCHING

Environment

Testing was conducted in high purity (99.9999%) hydrogen gas at a pressure of 55 MPa. The temperature in the autoclave was not controlled, however, the laboratory temperature is maintained at approximately 20˚C. Additional details of testing in gaseous hydrogen can be found in [14].

Fatigue and Fracture Test Methods

Compact tension specimens were extracted from the cylindrical body with two different orientations: T-L orientation with crack propagation direction parallel to the longitudinal axis of the vessel and T-R with crack propagation in the radial direction. Table 1 summarizes the sampling scheme and designation of test specimens. A total of six tests were conducted.

The specimen width was W = 26.4 mm and thickness B = 12.7 mm, following the designation in ASTM E647 and E1820. Side grooves were machined prior to precracking, reducing the thickness by about 12% (reduced thickness B_N = 11.2 mm nominally). Precracking was accomplished by shedding the maximum stress intensity factor (K_{max}) to less than 10 MPa $m^{½}$ at a final precrack length (a/W) of about 0.29.

Fatigue testing was conducted following the procedures of ASTM E647 with crack length determined in real-time by compliance measured from either load-line or front-face displacement and load applied on the specimen measured with a load cell inside the autoclave. The internal load cell was directly attached to the specimen and acting as the feedback transducer in the control loop.

For each specimen, fatigue cycling was conducted in K-control in several segments. Each segment was conducted at constant value of C^*, with subsequent segments alternating between positive and negative C^* (corresponding to increasing and decreasing dK/da conditions), where C^* is the normalized K-gradient given by:

$$C^* = \left(\frac{1}{K}\right)\left(\frac{\mathrm{d}K}{\mathrm{d}a}\right) \tag{6}$$

Tests were conducted without showing significant differences in the fatigue crack growth response for C^* values between ±0.39 mm^{-1} for the studied conditions. This approach was presented in previous publications and verified for load ratios between 0.1 to 0.7 as well as multiple K-gradients ([8], [15]). By testing subsequent segments with positive and negative C, multiple load ratio (R) values could be evaluated on the same specimen. An example of a test that evaluates three load ratios with a single specimen (ID: L3-1) is shown in Figure 3. In each of the segments, care was taken to ensure that crack growth was not significantly affected by the previous segment. This condition was determined by comparing data from K-increasing and K-decreasing segments (from same R) and maintaining $K_{max} \leq 30$ MPa $m^{1/2}$. Additionally, K_{max} is never stepwise decreased between segments; usually K_{max} is kept constant when transitioning from K-increasing to K-decreasing (as shown in Figure 3), although occasionally K_{max} is stepwise increased when transitioning between segments.

TABLE 1: SAMPLING ORIENTATION AND POSITION THROUGH THE THICKNESS

Specimen ID	Orientation	Sampling position
TT-RO-1	T-R	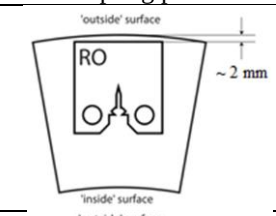
TT-RI-1	T-R	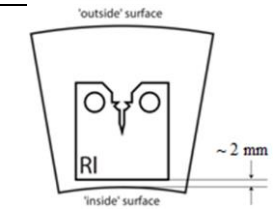
TT-L1-1 TT-L1-2	T-L	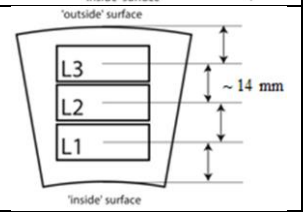
TT-L2-1	T-L	
TT-L3-1	T-L	

Most tests were conducted at frequency of 1 Hz as in previous publications [1], [8]. A few segments were evaluated at other frequencies (0.1 Hz 5 Hz, and 10 Hz), although a systematic study on the frequency effect was not the aim of the

work. As a general rule, frequency was chosen such that da/dt remained less than 10^{-6} m/s.

At the conclusion of the FCGR tests, FT tests were performed per the ASTM E1820 standard without removing the specimen from the autoclave. This procedure is permitted by concluding the fatigue test with a *K*-decreasing segment such that the final K_{max} is well below the material FT measured in the subsequent test and *a/W* is less than 0.7 (as shown in Figure 3). The load was increased monotonically during the FT at constant actuator displacement rate of approximately 0.005 mm/min, resulting in stress intensity factor variation (*K*-rate) less than 0.01 MPa $m^{½}$ s^{-1}.

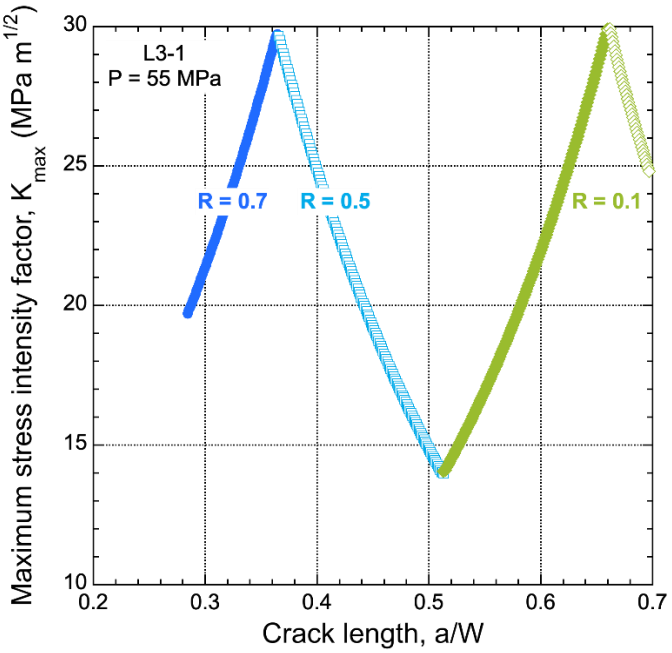

FIGURE 3: STRESS INTENSITY FACTOR AS A FUNCTION OF CRACK LENGTH FOR A SINGLE TEST SPECIMEN WITH FOUR FATIGUE TEST SEGMENTS. THE *K*-GRADIENT IS CONSTANT FOR EACH SEGMENT

DCPD was used to monitor crack length during the test, thus allowing an elastic-plastic fracture analysis according to ASTM E1820. In this manner, the *J*-value at the intersection of the 0.2 mm construction line was determined as J_{QH} (where the subscript *H* refers to testing in gaseous hydrogen). These values of *J* are converted to units of *K* as described in the standard and denoted K_{JQH} (plane strain modulus (E') of 227 GPa is assumed). Although the specimen size criteria are satisified per ASTM E1820, the criterion for straightness of the crack front is not always satisfied. These reported values are representative of plane strain fracture resistance despite nominal lack of straightness of the crack front in some cases (see Figure 4).

Figure 4 shows the fracture surface appearance at the end of the test for specimen ID: L3-1. Prior to breaking the specimen in two pieces, the specimen was heat tinted to mark the extent of crack extension during the FT test. The precracked area, the different segments for the FCGR test, and the region of stable crack extension during the FT test are indicated on the image (along with the post-test fracture in liquid nitrogen).

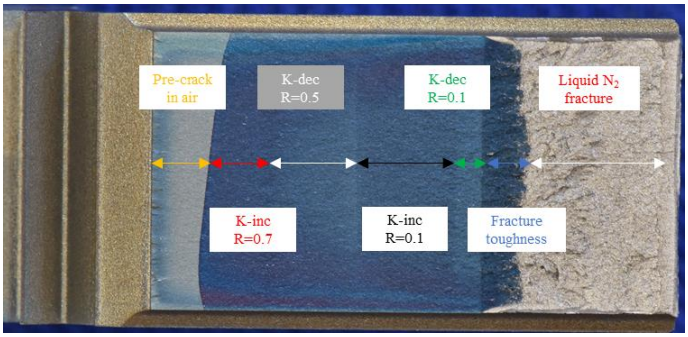

FIGURE 4: FRACTURE SURFACE APPEARANCE FOR SPECIMEN AFTER FATIGUE AND FRACTURE TEST IN H2. SEVERAL DISTINCT REGIONS CAN BE IDENTIFIED: PRECRACK (IN AIR), *K*-INCREASING AT *R*=0.7, *K*-DECREASING AT *R*=0.5, *K*-INCREASING AT *R*=0.1 AND *K*-DECREASING AT *R*=0.1, FT TEST, FOLLOWED BY LIQUID N_2 FRACTURE IN AIR TO OPEN SPECIMEN

3. FATIGUE AND FRACTURE TESTS RESULTS

Fracture Resistance

The measured fracture resistance data in 55 MPa gaseous hydrogen are given in Table 2. These new data show higher fracture resistance compared to existing data obtained at pressure above 100 MPa ([8]), confirming a pressure dependence of fracture resistance in hydrogen gas. Figure 5 shows the plots of crack extension resistance as a function of stable crack growth, also known as *J-R* curves, for all the specimens investigated. All specimens showed a ductile behavior with stable crack extension, also known as stable tearing, as per ASTM E1820 definition.

TABLE 2: SUMMARY OF ELASTIC-PLASTIC FRACTURE TOUGHNESS DATA MEASURED IN 55 MPA H_2 GAS

Specimen ID	J_{QH}	K_{JQH}
#	kJ/m^2	MPa $m^{½}$
L1-1	22.9	72.1
L1-2	28.8	80.9
L2-1	25.0	75.4
L3-1	27.8	79.5
RO-1	29.0	81.2
RI-1	28.2	80.1

Fatigue crack growth rate measurements

The measured FCGR in 55 MPa H_2 gas are shown in Figure 6, Figure 7, Figure 8 for load ratios *R*=0.1, *R*=0.5 and *R*=0.7, respectively. Each plot includes a dashed line showing the pressure corrected design curve as per Equation (4) for the lower ΔK regime, as well as the pressure independent portion of the design curve in the higher ΔK regime.

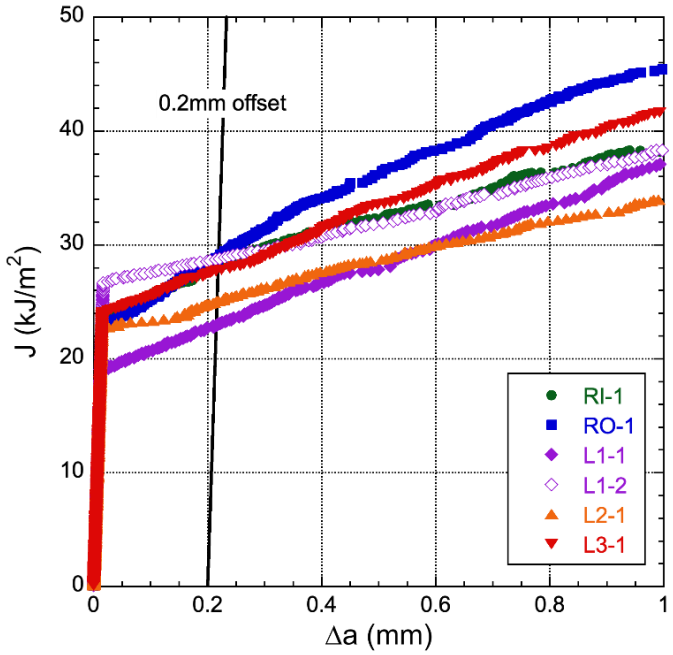

FIGURE 5: *J-R* CURVES GENERATED AT 55 MPa WITH THE OFFSET LINE AT 0.2 mm FOR THE DETERMINATION OF J_{QH}

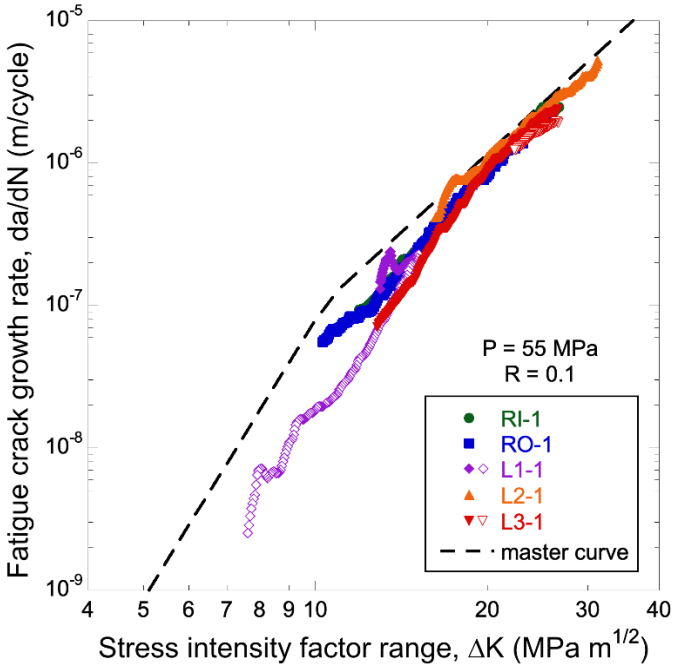

FIGURE 6: FCGR TESTS GENERATED AT 55 MPa AND R=0.1. CLOSED SYMBOLS ARE K-INCREASING, WHEREAS OPEN SYMBOLS ARE K-DECREASING. ALL TESTS PERFORMED WITH C^*= ±0.20 mm^{-1}

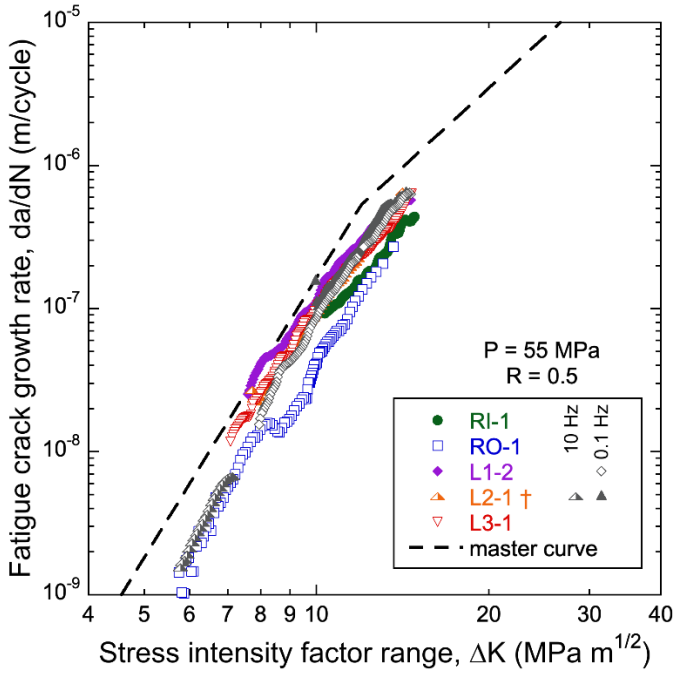

FIGURE 7: FCGR TESTS GENERATED AT 55 MPa AND R=0.5. CLOSED SYMBOLS ARE K-INCREASING, WHEREAS OPEN SYMBOLS ARE K-DECREASING. ALL TESTS PERFORMED WITH C^*= ±0.20 mm^{-1}, EXCEPT AS NOTED BY † WHERE C^* = -0.39 mm^{-1} FOR 0.1 Hz AND 10 Hz

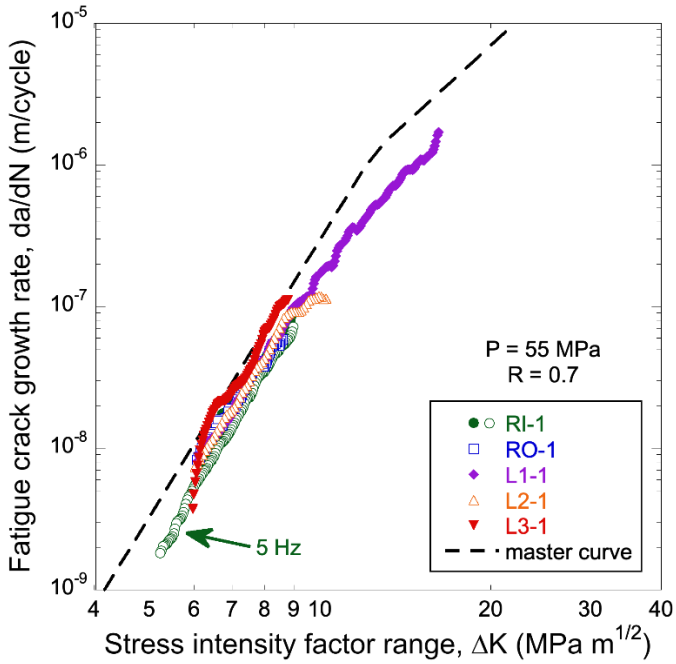

FIGURE 8: FCGR TESTS GENERATED AT 55 MPa AND R=0.7. CLOSED SYMBOLS ARE K-INCREASING, WHEREAS OPEN SYMBOLS ARE K-DECREASING. ALL TESTS PERFORMED WITH C^*= ±0.20 mm^{-1}, EXCEPT L2-1 WHERE C^* =-0.39 mm^{-1}

In all the tests, the design curves represent an upper bound fatigue rate with respect to the experimental tests, with additional conservatism in the low ΔK regime (despite the pressure correction). This conservativism is more evident for R=0.1 and R=0.5. The experimental data is well represented by the design curve in the pressure-independent (high ΔK) regime, demonstrating the lack sensitivity of FCGR to pressure (this correlation is most evident for R=0.1, Figure 6). There is no evidence of orientation dependence in these data: all specimens in this study show similar FCGR data despite extraction in different locations and orientations.

All the tests were conducted at 1 Hz except for a few segments where frequency was spanned from 0.1 Hz to 10 Hz. More specifically for R=0.5 (Figure 7), a more systematic evaluation of frequency was conducted with segments performed at 0.1 Hz and 10 Hz. From these tests a clear frequency effect is not recognized within the bounds of the resulting crack growth velocities (less than 10^{-6} m/s).

Additionally, as expected, FCGR for load ratios of R=0.1, R=0.5 and R=0.7 show a distinguishable difference and FCGR is clearly greater for higher load ratios. However, it is important to also recognize that, for a given applied ΔK, the K_{max} is substantially different depending on the applied load ratio. The relationship between K_{max} and ΔK is given in Equation (7):

$$K_{max} = \frac{\Delta K}{1-R} \tag{7}$$

At the same ΔK = 10 MPa $m^{½}$,the K_{max} is about 33.3 MPa $m^{½}$ for R=0.7, but 20 MPa $m^{½}$ for R=0.5 and only 11 MPa $m^{½}$ for R=0.1. Since hydrogen storage pressure vessels are designed to operate with a maximum pressure (hence a fixed K_{max} for a given flaw size), a deep pressure cycle (low R-ratio) will be more damaging than a shallow pressure cycle (high R-ratio), despite the fact that FCGR for high load ratios are higher than for low load ratios.

In the next section, a simple example of life assessment provides additional clarifications to this concept.

4. DISCUSSION

For pressures up to 21 MPa, FCGR of pipeline steels were found to be pressure dependent in the lower ΔK regime (but greater than threshold), and pressure independent in the higher ΔK regime [12], [15]. It is important to note that some prior publications showed a pressure dependency beyond the so-called "knee" point (i.e., the high ΔK region), characteristic of the master curve approach. Macadre and co-authors ([9]) studied the effect of hydrogen gas pressure at 0.7 MPa and 90 MPa on a Q&T SNCM 439 (Ni-Cr-Mo) steel tested under decreasing ΔK conditions at R=0.5, showing a significant hydrogen pressure effect even in the upper ΔK regime. Yamabe and co-authors ([16]) investigated the effect of four different hydrogen gas pressures, 0.7 MPa, 10 MPa, 40 MPa, and 90 MPa on a Q&T SCM 435 tested at R=0.1 and they found little difference in the high ΔK regime from 0.7 MPa to 40 MPa, but a slight increase in FCGR at 90 MPa. However, in the high ΔK regime, the upper bound FCGR curves are consistent with the master curve approach presented in the current work and in previous publication [1]. San Marchi and co-authors performed FCGR tests on a 4130X (Cr-Mo steel) in 45 MPa hydrogen gas pressure at R=0.1 [17]. Comparison of these data with the present work shows consistent results in the high ΔK region (e.g little or no pressure dependency), although insufficient data are available for a full evaluation in the low ΔK regime.

Fracture properties are also known to be dependent on the hydrogen gas pressure, with hydrogen reducing fracture toughness even for low gas pressure (< 0.1 MPa) as shown in [18]. However, the effect of hydrogen gas pressure becomes less important as pressure increases, showing a relatively mild dependence on fugacity for high-pressure conditions [12]. Yamabe et al. [16] investigated a Q&T Cr-Mo steel with tensile strength of 830 MPa and found a K_{JH} value of approximately 160 MPa $m^{½}$ at 45 MPa hydrogen gas pressure. This result is significantly higher compared to the values found in the present work. Similar, high values are reported by Iijima and coworkers [19], on a SA372 Gr. J tested at 45 MPa hydrogen gas pressure, while tests at 115 MPa pressure are consistent with previously available data [8] on the A372 Grade N Class 100 material investigated in this work.

ASME CC2938-1 allows using the master curves up to K_{max} = 40 MPa $m^{½}$, thus enforcing a conservative lower bound for fracture toughness. Results of this study suggests that a higher K_{max} could be allowed based on the fracture properties measured at 55 MPa. A higher fracture resistance has implications also on the fatigue behavior since, as K_{max} during a fatigue test approaches K_{JH}, a transition to stage III is observed, where the FCGR curve no longer follows the traditional power law dependence on ΔK (i.e., the log(da/dN)-log(ΔK) curve displays an increasing slope – see [8]).

Although an increase in allowable K_{max} would likely not result in significant benefits on the resulting number of cycles to failure (at high K_{max}, a crack grows very quickly and thus the additional number of cycles would be minor), further data on the dependence of fracture toughness on pressure may provide additional insights for the prediction and calculation of LBB in hydrogen gas, which remains a topic not fully documented.

In the next section, a simple life assessment example is presented with the aim to reveal the benefits of using pressure corrected FCGR to reduce conservatism in design.

Example of life assessment

The following assessment demonstrates the potential benefit of fracture mechanics assessments for service life prediction of hydrogen pressure vessels. Additionally, the effect of the pressure-correction (as described in the introduction) is evaluated. In this example, a cylindrical pressure vessel with 360 mm OD × 48.5 mm minimum WT is considered.

Two different scenarios are investigated:

1. A deep pressure cycle from a maximum pressure of 55 MPa to a minimum pressure of 5.5 MPa, corresponding to a load ratio R=0.1.

2. A shallow pressure cycle from a maximum pressure of 55 MPa to a minimum pressure of 27.5 MPa corresponding to a load ratio R=0.5.

For this assessment, an initial thumbnail flaw was assumed with a depth (a) equal to 1 mm on the inside surface and a depth to length ratio, $a/2c$ = 1/3, aligned with the longitudinal axis of the cylindrical vessel. The stress intensity factor for this flaw was determined using existing solutions given in API 579-1/ASME FFS-1 [20]. For each of the above scenarios, calculations were performed using FCGR as per CC2938-1 and FCGR corrected for 55 MPa hydrogen gas as per Equation (4). For simplicity, the maximum value for K was limited to 40 MPa $m^{½}$ as in the current ASME CC 2938-1, so no additional credit was taken for the higher fracture values reported in Table 2.

The allowable crack size and number of cycles were calculated using the FAD as given in API 579-1/ASME FFS-1. Table 3 provides a summary of the results in terms of the predicted number of cycles to failures for each of the investigated conditions. The use of pressure corrected FCGR curves, expectedly, predicts additional cycles to failure compared to the standard FCGR as per CC2938-1.

TABLE 3: EXAMPLE OF LIFETIME CALCULATION FOR A VESSEL WITH MAXIMUM OPERATING PRESSURE 55 MPA. COMPARISON OF PREDICTED NUMBER OF CYCLES CONSIDERING CC2938-1 CURVES AND PRESSURE CORRECTED FCGR CURVES

Predicted Number of Cycles to Failure		
	Per current CC2938-1	Pressure corrected to 55 MPa (Equation 4)
Scenario 1: deep cycle ΔP = 55-5.5 MPa (R=0.1)	19,000	19,800
Scenario 2: shallow cycle ΔP = 55-27.5 MPa (R=0.5)	158,000	243,000

The benefit becomes more evident for the shallow pressure range (R=0.5) as the estimated initial applied ΔK is approximately 5.3 MPa $m^{½}$, while it is about 9.5 MPa $m^{½}$ for the deep pressure range (R=0.1).

Figure 9 helps to visualize this concept: given a fixed K_{max}, corresponding to a maximum design pressure, the initial applied ΔK is lower for a higher R ratio (R=0.5), meaning that a larger portion of crack life is spent in the region where FCGR is lowered based on Equation (4).

Above the transition point, in the upper ΔK region, there is no benefit of pressure correction and this explains the smaller difference in Table 3 obtained for R=0.1, as the initial applied ΔK is relatively close to this transition.

In summary, for a shallow pressure cycle (lower initial ΔK at higher R, recall Equation 7), the design life prediction benefits from a lower initial FCGR in the pressure dependent regime. In contrast, for the deeper pressure cycle, (greater ΔK for the same K_{max}, thus lower R), the resulting FCGR is independent of pressure from the onset of life (recall Figure 1). In other words, and as shown by this simple example, a pressure correction to existing CC2938-1 has significant benefit for pressure vessels designed to shallower pressure cycles (higher R). This benefit of accounting for pressure-dependent in FCGR is significantly less for vessel designs with deep pressure cycles (i.e., R approaching zero).

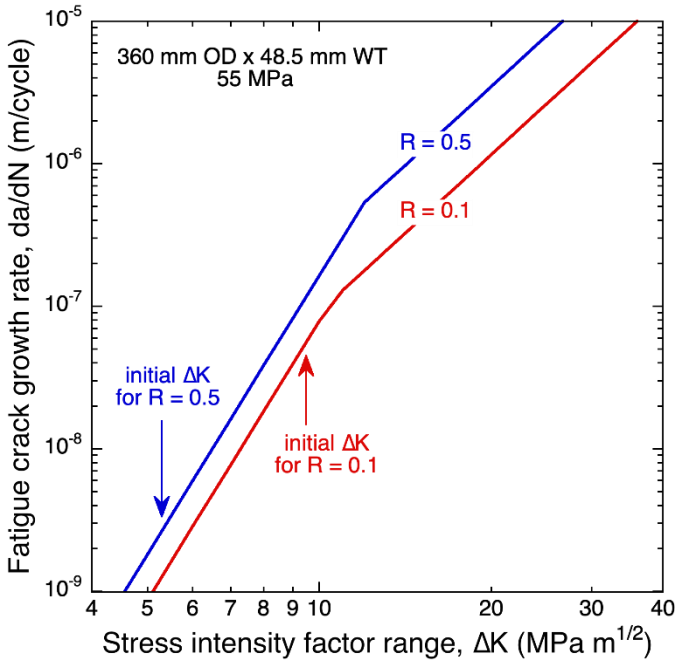

FIGURE 9: INITIAL APPLIED ΔK FOR LOAD RATIO R=0.1 AND R=0.5 USED IN THE LIFE ASSESSMENT EXAMPLE. HIGHER R RATIO (R=0.5) IMPLIES LOWER INITIAL APPLIED ΔK RESULTING IN LARGER NUMBER OF CYCLES TO FAILURE

5. CONCLUSION

This study presents FCGR and FT data measured in gaseous hydrogen at pressure of 55 MPa from a Q&T A372 Grade N (Ni-Cr-Mo) Class 100 steel. Extraction and testing of several orientations and locations in the thick-walled vessel revealed that the FCGR response was nominally independent of these variables.

Acquisition of FCGR data was accelerated through K-controlled testing utilizing both K-increasing and K-decreasing segments in a single test specimen, enabling multiple load ratios in each test. Additionally, this methodology facilitated testing at relatively low ΔK, which emphasized the effect of hydrogen pressure on FCGR at low ΔK. In contrast, at high ΔK, FCGR is remarkably insensitive to hydrogen partial pressure.

The existing ASME CC 2938-1 offers a simple da/dN vs ΔK relationship for Cr-Mo and Ni-Cr-Mo steels, providing upper bound FCGR curves that can be used for the design of pressure vessels up to 103 MPa (15,000 psi). These curves were originally

derived from tests conducted at pressure of 106 MPa. The FCGR data in this study are significantly lower than CC2938-1 at low ΔK, but can be captured by a simple pressure correction, based on the fugacity concept as shown in Equation (4). Comparison of fatigue design life predictions utilizing the CC2938-1 curves and pressure-corrected FCGR curves respectively reveals a substantially extended design life for cascade storage systems (meaning the pressure ratio in the vessel, represented by the mechanical variable R, is close to or greater than 0.5).

A similar pressure correction factor for fracture toughness would also be desirable and would allow higher K values in fracture mechanics calculation, whereas the existing CC2938-1 is limited to $K_{max} = 40$ MPa $m^{½}$. However, it should be noted that higher K values would have little benefit from a life assessment perspective, as cracks grow very quickly in the upper ΔK region, such that the additional design life would be modest.

ACKNOWLEDGEMENTS

This article has been authored by an employee of National Technology & Engineering Solutions of Sandia, LLC under Contract No. DE-NA0003525 with the U.S. Department of Energy (DOE). The employee owns all right, title and interest in and to the article and is solely responsible for its contents. The United States Government retains and the publisher, by accepting the article for publication, acknowledges that the United States Government retains a non-exclusive, paid-up, irrevocable, world-wide license to publish or reproduce the published form of this article or allow others to do so, for United States Government purposes. The DOE will provide public access to these results of federally sponsored research in accordance with the DOE Public Access Plan https://www.energy.gov/downloads/doe-public-access-plan.
This paper describes objective technical results and analysis. Any subjective views or opinions that might be expressed in the paper do not necessarily represent the views of the U.S. Department of Energy or the United States Government.

REFERENCES

[1] San Marchi C, Ronevich J., Bortot P., Wada Y., Felbaum J., Rana M., Technical basis for master curve for fatigue crack growth of ferritic steels in high-pressure gaseous hydrogen in ASME Section VIII-3 code (PVP2019-93907), ASME Pressure Vessels & Piping Conference, San Antonio, TX, 2019.

[2] Gaseous Hydrogen Embrittlement of Materials in Energy Technologies, Editors: R. Gangloff, B.P. Somerday, Woodhead Publishing, 2012.

[3] San Marchi C., Somerday B.P., Technical Reference for Hydrogen Compatibility of Materials. Report no. SAND2012-7321. Sandia National Labs, 2012.

[4] Loginow A.W., Phelps E.H., Steels for Seamless Hydrogen Pressure Vessels. Corrosion 31 (1975) 404-12.

[5] Wada Y., Ishigaki R., Tanaka Y., Iwadata T., Ohnishi K., Effect of hydrogen gas pressure on the mechanical properties of low alloy steel for hydrogen pressure vessels (PVP2007-26553), ASME Pressure Vessels and Piping Conference, San Antonio TX, 2007.

[6] Nibur K.A., San Marchi C., Somerday B.P., Fracture and fatigue tolerant steel pressure vessels for gaseous hydrogen (PVP2010-25827), ASME Pressure Vessels and Piping Conference, Bellevue WA, 2010.

[7] Ronevich J.A., San Marchi C., Brooks D., Emery J.M., Grimmer P., Chant E., Exploring life extension opportunities of high pressure hydrogen pressure vessels at refueling stations (PVP2021-61815), ASME Pressure Vessel and Piping Conference; virtual, 2021.

[8] San Marchi C., Bortot P., Wada Y., Ronevich J.A., Fatigue and fracture of high-hardenability steels for thick-walled hydrogen pressure vessels. International Conference on Hydrogen Safety (ICHS), Hamburg, Germany, 2017.

[9] Macadre, M., Artamonov, M., Matsuoka, S., and Furtado, J., Effects of Hydrogen Pressure and Test Frequency on Fatigue Crack Growth Properties of Ni-Cr-Mo Steel Candidate for a Storage Cylinder of a 70 MPa Hydrogen Filling Station, Eng. Fract. Mech., 78(18), 2011, 3196-3211.

[10] Somerday B.P., Bortot P., Felbaum J., Optimizing measurement of fatigue crack growth relationships for CrMo pressure vessel steels in hydrogen gas (PVP2015-45424), ASME Pressure Vessels and Piping Conference, Boston MA, 2015.

[11] San Marchi C., Somerday B.P., Robinson S.L., Permeability, Solubility and Diffusivity of Hydrogen Isotopes in Stainless Steels at High Gas Pressure, International Journal of Hydrogen Energy, Volume 32, 2007, 100-116.

[12] Ronevich J.A., San Marchi C., Materials compatibility concerns for hydrogen blended into natural gas (PVP2021-62045), ASME Pressure Vessels and Piping Conference; virtual, 2021.

[13] ASTM A372/A372M-20, Standard Specification for Carbon and Alloy Steel Forgings for Thin-Walled Pressure Vessels.

[14] Somerday B.P., Campbell J.A., Lee K.L., Ronevich J., San Marchi C., Enhancing safety of hydrogen containment components through materials testing under in-service conditions, International Journal of Hydrogen Energy, Volume 42, 2017, 7314-7321.

[15] Ronevich J.A., San Marchi C., Fatigue and Fracture of Pipeline Steels in high-pressure Hydrogen Gas (PVP2022-85757), ASME Pressure Vessels and Piping Conference, Las Vegas NV, 2022.

[16] Yamabe J., Itoga H., Awane T., Matsuo T., Matsunaga H., Matsuoka S., Pressure Cycle Testing of Cr–Mo Steel Pressure Vessels Subjected to Gaseous Hydrogen, Journal of Pressure Vessel Technology, Vol. 138, 2016.

[17] San Marchi C., Harris A., Yip M., Somerday B.P., Pressure cycling of steel pressure vessels with gaseous hydrogen (PVP2012-78709), ASME Pressure Vessels and Piping Conference, San Antonio TX, 2007.

[18] Briottet L., Ez-Zaki, H., Influence of hydrogen and oxygen impurity content in a natural gas / hydrogen blend on the toughness of an API X70 steel (PVP2018-84658), ASME

Pressure Vessel and Piping Division Conference, Prague, Czech Republic, 2018.

[19] Iijima T., Itoga H., An B., San Marchi C., Somerday B.P., Measurement of fracture properties for ferritic steels in high pressure hydrogen gas, (PVP2014-28815), ASME Pressure Vessels and Piping Conference, Anaheim, CA, USA, 2014.

[20] API 579-1/ASME FFS-1 2021 Fitness-For-Service Code.